

## ***In Vivo* Quantification of Blood Flow and Wall Shear Stress in the Human Abdominal Aorta During Lower Limb Exercise**

CHARLES A. TAYLOR,<sup>1,2</sup> CHRISTOPHER P. CHENG,<sup>2</sup> LEANDRO A. ESPINOSA,<sup>2</sup> BEVERLY T. TANG,<sup>2</sup>  
DAVID PARKER,<sup>2</sup> and ROBERT J. HERFKENS<sup>3</sup>

<sup>1</sup>Department of Surgery, <sup>2</sup>Department of Mechanical Engineering, and <sup>3</sup>Department of Radiology, Stanford University, Stanford, CA

(Received 9 December 2001; accepted 19 February 2002)

**Abstract**—Magnetic resonance (MR) imaging techniques and a custom MR-compatible exercise bicycle were used to measure, *in vivo*, the effects of exercise on hemodynamic conditions in the abdominal aorta of eleven young, healthy subjects. Heart rate increased from  $73 \pm 6.2$  beats/min at rest to  $110 \pm 8.8$  beats/min during exercise ( $p < 0.0001$ ). The total blood flow through the abdominal aorta increased from  $2.9 \pm 0.6$  L/min at rest to  $7.2 \pm 1.4$  L/min during exercise ( $p < 0.0005$ ) while blood flow to the digestive and renal circulations decreased from  $2.1 \pm 0.5$  L/min at rest to  $1.6 \pm 0.7$  L/min during exercise ( $p < 0.01$ ). Infrarenal blood flow increased from  $0.9 \pm 0.4$  L/min at rest to  $5.6 \pm 1.1$  L/min during exercise ( $p < 0.0005$ ). Wall shear stress increased in the supraceliac aorta from  $3.5 \pm 0.8$  dyn/cm<sup>2</sup> at rest to  $6.2 \pm 0.5$  dyn/cm<sup>2</sup> during exercise ( $p < 0.0005$ ) and increased in the infrarenal aorta from  $1.3 \pm 0.8$  dyn/cm<sup>2</sup> at rest to  $5.2 \pm 1.3$  dyn/cm<sup>2</sup> during exercise ( $p < 0.0005$ ). © 2002 Biomedical Engineering Society. [DOI: 10.1114/1.1476016]

**Keywords**—Magnetic resonance imaging, Blood flow distribution, Lower limb exercise, Shear stress, Flow rate, Atherosclerosis, Hemodynamics.

### **INTRODUCTION**

Hemodynamic factors including shear stress, cyclic strain, and pressure forces play an important role in the normal adaptive response of blood vessels to chronic changes in physiologic demands and in maladaptive responses leading to cardiovascular disease. In particular, it is hypothesized that flow recirculation, high particle residence time, and low mean wall shear stress are responsible for the localization of atherosclerotic plaques in regions of complex flow in the carotid bifurcation, coronary arteries and abdominal aorta.<sup>1,7,10,36</sup> These low shear areas are hypothesized to be more susceptible to cholesterol accumulation due to low local diffusional efflux from the arterial wall to blood and enhanced monocyte binding.<sup>1,4</sup> In contrast to the effects of low shear stress, it

has been shown that chronic increases in blood flow stimulates the expression of nitric oxide synthase and (Cu/Zn) superoxide dismutase that reduces the concentration of cellular superoxide anion ( $O_2^-$ ), as well as the expression of monocyte chemoattractant protein-1 and vascular cell adhesion molecule-1.<sup>4,17</sup> These effects are hypothesized to reduce the endothelial adhesiveness of monocytes and protect the vascular endothelium from atherosclerotic plaques. In addition, elevated shear stress induces direct cellular structural changes including cell elongation in the direction of maximum stress and results in inhibition of atherosclerosis.<sup>35</sup>

Exercise is one important mechanism that increases blood flow and wall shear stress; however, all the vessels of the body do not experience these changes uniformly. The regions of the vasculature that experience increased blood flow and wall shear stress during exercise may enjoy some of the protection from atherosclerotic plaques observed with chronic increases in blood flow. Even short bouts of exercise can lead to biological changes in arteries exposed to increased blood flow and elevated shear stress and may influence cardiovascular fitness even after the cessation of physical activity. Wang *et al.* found that bouts of exercise enhanced acetylcholine-induced dilation of the large coronary artery in dogs and hypothesized that this was due to the increased levels of endothelium relaxation factor/nitric oxide (EDRF/NO).<sup>32</sup> Furthermore, the enhanced coronary vasodilation and increased release of EDRF/NO is hypothesized to be due to the upregulation of NO in the coronary vascular endothelial cells. Sessa *et al.* determined that chronic exercise in dogs increases endothelial cell nitric oxide synthase gene expression.<sup>27</sup> Thus, in addition to the widely known systemic benefits achieved with exercise, e.g., enhanced cholesterol metabolism and lower blood pressure, increased blood flow and wall shear stress may provide localized benefits for cardiovascular health.

For the aorta, although systemic risk factors for arterial disease, such as hypertension, diabetes, sedentary

Address correspondence to: Charles A. Taylor, Division of Biomechanical Engineering, Durand Building, Room 213, Stanford, CA 94305-3030. Electronic mail: taylorca@stanford.edu

lifestyle, cigarette smoking, and genetic disposition affect the thoracic and abdominal aorta equally, atherosclerosis is observed with more frequency and greater severity in the abdominal aorta than in the thoracic aorta.<sup>8,25</sup> Computational, *in vitro*, and *in vivo* studies have shown that these lesion-prone locations of the human aorta coincide with regions of flow recirculation, high particle residence time, and low wall shear stress.<sup>11–15,20,30,31</sup> Computational<sup>31</sup> and *in vitro* studies<sup>11,13</sup> have shown that these adverse hemodynamic conditions are significantly reduced by increased blood flow into the distal abdominal aorta, a well-known effect of lower limb exercise. However, computational and *in vitro* investigations utilize simplifying assumptions and rely on the specification of the blood flow distribution between the digestive, renal and lower extremity circulations.

We previously reported changes in blood flow in the abdominal aorta during very light exercise conditions in a conventional magnetic resonance imager using a custom leg flexion and extension device.<sup>26</sup> Niezen *et al.*<sup>16</sup> previously measured blood flow during exercise in the ascending aorta and pulmonary artery under very light exercise conditions using magnetic resonance imaging. Pedersen *et al.*<sup>21</sup> measured changes in blood flow rate immediately after light and moderate exercise using a breath-held magnetic resonance imaging (MRI) technique. In all cases, including our own measurements, exercise was performed in a supine position and shear stress or oscillatory shear stress was not reported. Furthermore, the effect of exercise conditions on flow distribution between the lower extremities and the digestive and renal circulations has not been previously reported.

We have utilized a custom MR-compatible bicycle in a 0.5 T open magnet (GE Signa SP, GE Medical Systems, Milwaukee, WI) (Fig. 1) and cine phase contrast MRI (cine PC-MRI) techniques<sup>23</sup> to measure, *in vivo*, the spatial distribution of blood flow velocities in the abdominal aorta of human subjects during upright rest and light exercise conditions. By integrating the through-plane velocity over the vessel cross section, flow rates can be calculated. Furthermore, shear stresses are quantified by differentiating the blood flow velocity field, and assuming a constant blood viscosity. We report the effect of exercise conditions on volume flow rate, flow distribution between the lower extremities and the digestive (foregut and midgut) and renal circulations, flow temporal oscillations, mean wall shear stress, and shear stress temporal oscillations in the human abdominal aorta.

## METHODS

Eleven healthy, normal subjects [six males, median age 22.5 years (20–24 years) and five females, median age 24 years (23–28 years)] were imaged during rest and exercise. Strong *et al.* found that less than 4% of a rep-



**FIGURE 1.** Subject pedaling on MR-compatible bicycle in 0.5 T open magnet.

resentative population with the same age profile experience hemodynamically significant atherosclerotic lesions.<sup>29</sup> Each subject was securely strapped to a seat in the open magnet such that they had the full range of leg motion while being positioned to obtain the highest signal to noise ratio and contrast in the abdominal region. The bicycle was then positioned and the pedal resistance was set to minimize abdomen movement. Figure 1 depicts a subject cycling in the magnet.

Scans were performed at rest and during steady-state exercise conditions (150% of resting heart rate) within the range of light exercise (35%–59% of maxHR).<sup>24</sup> In order to maintain this level of exercise, the subjects monitored their own heart rate (heart rate was displayed in real-time on the pulse monitor) and adjusted pedaling speed as necessary to maintain a constant heart rate.

Cine PC-MRI techniques were used to measure through-plane blood flow velocity as a function of position at the supraceliac, suprarenal, and infrarenal levels at rest and during exercise as shown in Fig. 2.<sup>23</sup> The image acquisitions were gated to the cardiac cycle using a plethysmograph, and data was retrospectively reconstructed at 16 discrete time points within the cardiac cycle irrespective of RR interval. Patients breathed normally during the acquisitions and respiratory compensation algorithms were utilized.<sup>6</sup> Scan parameters included a 25 ms TR, a 9 ms TE, a 30° flip angle, a 5 or 10 mm

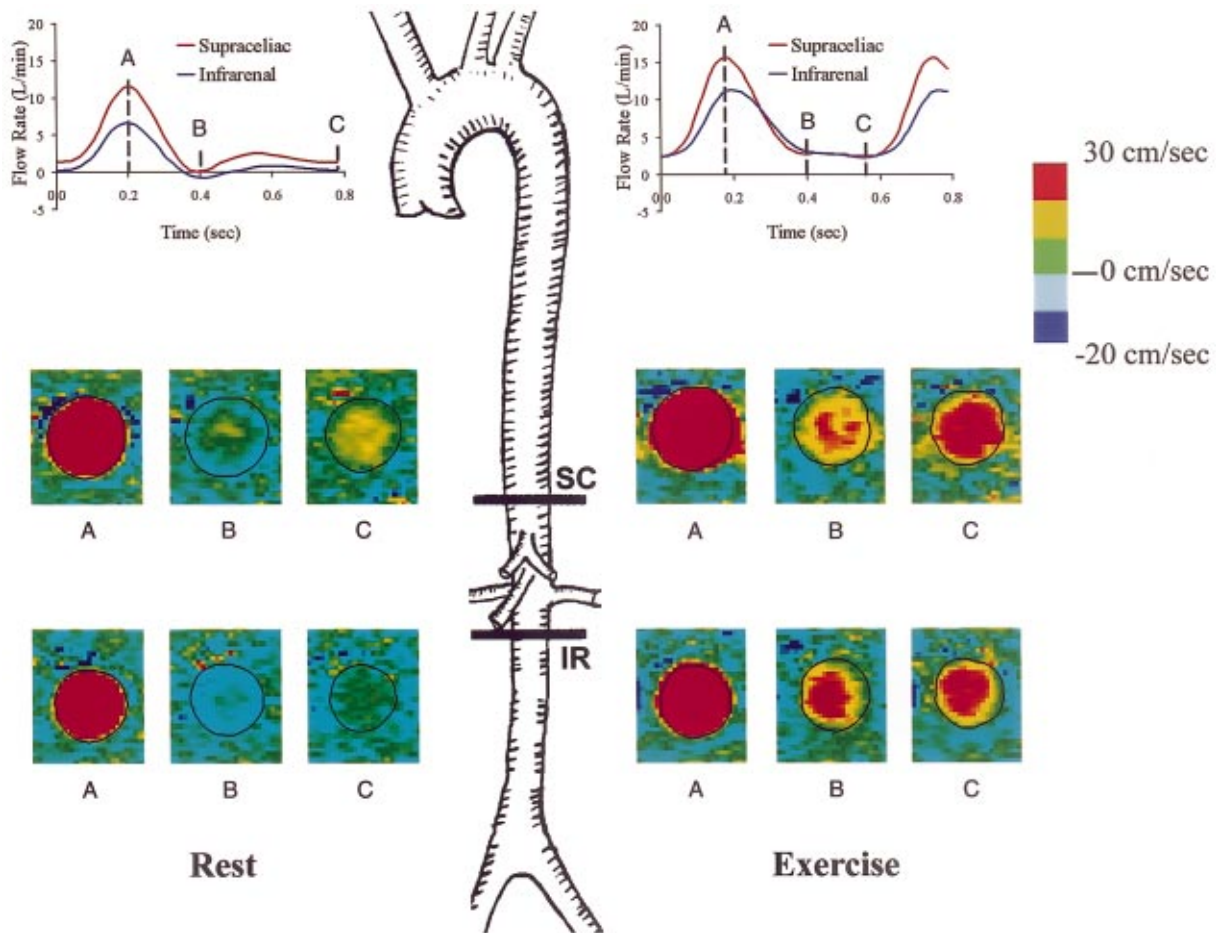


**FIGURE 2.** Schematic of human aorta, measured flow rate and velocity data for representative subject at rest (left) and during dynamic exercise (right). The celiac, superior mesenteric and renal arteries are depicted between the supraceliac (SC) and infrarenal (IR) image planes. The suprarenal image plane (not shown) was located between the superior mesenteric and renal arteries. Volume flow rate curves demonstrate reversal of flow in the infrarenal aorta under resting conditions and significant increase in flow rate with exercise. Contours of measured velocity data are depicted in the supraceliac (top) and infrarenal aorta (bottom) at rest (left) and exercise (right) at three times during the cardiac cycle. Also shown are the inner boundaries of the aorta identified by segmenting the MR magnitude data. The supraceliac contour plots demonstrate the significant increase in blood flow entering the abdominal aorta with lower limb exercise. The infrarenal contour plots demonstrate flow reversal and stasis (negative or low velocity) during diastole at rest (times B and C) and positive forward flow throughout the cardiac cycle under exercise conditions.

slice thickness (to maximize signal depending on the anatomy of the subject), a 28 cm square field of view, a 256 by 128 matrix, and a 150 cm/s through-plane velocity encoding gradient. For the three levels of the aorta we obtained sets of spatial maps of magnitude and velocity that describe the anatomy and blood flow at that location. These sets of 16 images, which represent an “average” cardiac cycle, were acquired over a period of 256 real-time heartbeats. With the cross section of the aorta of a particular slice isolated by image segmentation of the intensity data, blood flow velocity values (corrected for background signal) were assigned to each pixel within that cross section, multiplied by the area of a pixel, and summed to calculate total volume flow rate.<sup>22</sup>

The volume flow at the supraceliac level represents the total blood flow into the abdominal aorta, while the majority of infrarenal flow supplies the lower extremities and pelvic region. By subtracting the flow through the infrarenal slice from the flow at the supraceliac slice, combined blood flow to the foregut, midgut and renal circulations was determined. In order to quantify temporal oscillations in flow rate, we defined an oscillatory flow index (OFI) as

$$\text{OFI} = \frac{1}{2} \left( 1 - \frac{\int_0^T Q dt}{\int_0^T |Q| dt} \right),$$

where  $T$  is the period of the cardiac cycle. Note that an oscillatory flow index of zero corresponds to a positive flow rate through the vessel throughout the cardiac cycle whereas an oscillatory flow index of 0.5 corresponds to a net mean flow rate of zero over the cardiac cycle.

In order to compute shear stress, an accurate representation of the vessel boundary is needed. We used a level set method to segment the magnetic resonance intensity data and identify the curve  $C$  defining the intersection between the inner surface of the vessel and the imaging plane.<sup>28,33</sup> Shear stress  $\tau$  was computed along this curve using the gradient of the measured velocity data and the equation

$$\tau = \mu \left( \frac{\partial v}{\partial x} n_x + \frac{\partial v}{\partial y} n_y \right),$$

where  $v$  is the blood velocity normal to the image plane,  $(n_x, n_y)$  are the components of a vector normal to the curve  $C$ , and  $\mu$  is the dynamic viscosity of the blood.<sup>2,3</sup> To compute the velocity gradient along the curve,  $C$ , we construct a band of two-dimensional elements along the inside of this curve. Velocities are approximated on this band using cubic Lagrange polynomial interpolation functions. The nodes on the Lagrange polynomial elements are assigned velocity values computed from bicubic interpolation of the phase-contrast velocity values of the surrounding image pixels. For each element node, the 16 adjacent pixels of the MR velocity image are used for interpolation. The velocities of the pixels outside of the segmentation are set to zero. Once the nodal velocity values are assigned, the velocity at any point on the element can be computed as the sum of the products of the Lagrange interpolation functions evaluated at this point and the corresponding nodal velocity values. Velocity gradients are calculated and evaluated along the luminal curve and shear stress computed. Average shear stress along the luminal curve is calculated by integrating the shear stress along this curve and dividing by the circumference of the vessel. A mean shear stress averaged over this luminal curve and time is computed and presented. We have validated this approach using software phantoms and *in vitro* data and shown that we can reliably compute mean shear stress for pulsatile flow at the resolutions utilized in the present investigation.<sup>2,3</sup> Finally, to quantify temporal oscillations in shear stress, we defined the OSI<sup>9</sup> as

$$\text{OSI} = \frac{1}{2} \left( 1 - \frac{\int_0^T \tau dt}{\int_0^T |\tau| dt} \right).$$

Note the similarities with the oscillatory flow index.

## RESULTS

In this experiment, heart rate increased from  $73 \pm 6.2$  beats/min at rest to  $110 \pm 8.8$  beats/min during exercise ( $p < 0.0001$ ). The change in heart rate and increased metabolic demand in the lower limbs during exercise resulted in significant changes in blood flow in the abdominal aorta. Figure 2 depicts the supraceliac and infrarenal volumetric flow and through-plane velocity data for a representative subject. Under resting conditions, the supraceliac flow rate is positive throughout the cardiac cycle although it does approach zero in early diastole. In the infrarenal aorta, a period of reverse flow is observed in early diastole and the volumetric flow is nearly zero throughout the remainder of diastole. The velocity data reveals that, consistent with pulsatile flow theory, the reversal of flow occurs near the lumen boundary. Under exercise conditions, the volumetric flow rate at both the supraceliac and infrarenal levels are significantly elevated and positive throughout the cardiac cycle. The contour plots reveal positive blood flow velocities throughout diastole at both the supraceliac and infrarenal levels under exercise conditions.

The total blood flow through the abdominal aorta (as measured in the supraceliac aorta) increased from  $2.9 \pm 0.6$  L/min at rest to  $7.2 \pm 1.4$  L/min during exercise ( $p < 0.0005$ ), the blood flow to the digestive (foregut and midgut) and renal circulations decreased from  $2.1 \pm 0.5$  L/min at rest to  $1.6 \pm 0.7$  L/min during exercise ( $p < 0.01$ ), and the infrarenal blood flow increased from  $0.9 \pm 0.4$  L/min at rest to  $5.6 \pm 1.1$  L/min during exercise ( $p < 0.0005$ ) [Fig. 3(a)]. It is of note that, on average, less than 30% of the total abdominal aorta blood flow continues into the infrarenal aorta under resting conditions, while under exercise conditions this increases to nearly 80%. Flow reversal, as measured by the oscillatory flow index, was observed in the infrarenal aorta at rest and was eliminated with exercise [Fig. 3(b)]. Mean wall shear stress increased in the supraceliac aorta from  $3.5 \pm 0.8$  dyn/cm<sup>2</sup> at rest to  $6.2 \pm 0.5$  dyn/cm<sup>2</sup> during exercise ( $p < 0.0005$ ) and increased in the infrarenal aorta from  $1.3 \pm 0.6$  dyn/cm<sup>2</sup> at rest to  $5.2 \pm 1.3$  dyn/cm<sup>2</sup> during exercise ( $p < 0.0005$ ) [Fig. 3(c)]. The OSI was zero in the supraceliac aorta at rest and during exercise and decreased in the infrarenal aorta from  $0.1 \pm 0.1$  at rest to zero during exercise ( $p < 0.0001$ ) [Fig. 3(d)].

## DISCUSSION

Data from all subjects revealed that, in addition to the obvious fact that lower limb exercise conditions result in an increase in the total blood flow entering the abdominal aorta, flow oscillations, mean shear stress and oscil-

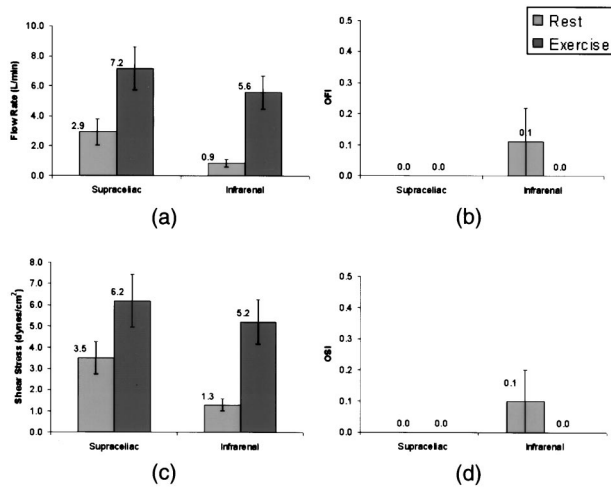


**FIGURE 3.** Comparison of hemodynamic conditions in supraceliac and infrarenal aorta under resting and exercise conditions showing (a) volumetric flow rate, (b) OFI, (c) mean shear stress, and (d) oscillatory shear index. The differences between rest and exercise were all highly statistically significant ( $p < 0.0005$ ). Note that, as shown in (b), the oscillatory flow index was identically zero in the supraceliac and infrarenal aorta under exercise conditions.

lations in shear stress were significantly altered. As blood flow increased due to exercise, flow oscillations observed at rest in the infrarenal aorta disappeared, supraceliac and infrarenal shear stress was significantly elevated and temporal oscillations in shear stress vanished.

Prior computational and *in vitro* studies using idealized models obtained comparable qualitative and quantitative results.<sup>12,13,31</sup> Under resting conditions, the mean shear stress was measured to be  $3.5 \pm 0.8$  dyn/cm<sup>2</sup> at the supraceliac level and  $1.3 \pm 0.6$  dyn/cm<sup>2</sup> at the infrarenal level in the present study. Moore *et al.*<sup>15</sup> measured the shear stress at the supraceliac level to be  $1.3 \pm 0.6$  dyn/cm<sup>2</sup> in an *in vitro* study with approximately the same abdominal aorta flow as measured in this study. We previously published computational simulations of blood flow in the abdominal aorta and reported mean shear stress at the supraceliac level on the order of 1–2 dyn/cm<sup>2</sup> and less than 1 dyn/cm<sup>2</sup> in the infrarenal aorta under resting conditions.<sup>30,31</sup>

Prior *in vivo* investigations under resting conditions have reported abdominal aorta shear stress values higher than those we report in the present investigation. Oshinski *et al.* used cine PC-MRI to measure flow velocity in the abdominal aorta under resting conditions and computed shear stress using a linear fit to the near wall velocity data.<sup>18</sup> They reported shear stress values of  $8.6 \pm 3.2$  dyn/cm<sup>2</sup> along the anterior wall and  $10.4 \pm 2.9$  dyn/cm<sup>2</sup> along the posterior wall at the suprarenal level.<sup>18</sup> At the infrarenal level they measured shear stress values of  $6.1 \pm 2.6$  dyn/cm<sup>2</sup> along the anterior wall and

$4.7 \pm 2.6$  dyn/cm<sup>2</sup> along the posterior wall.<sup>18</sup> Oyre *et al.*<sup>19</sup> also reported shear stress values in the abdominal aorta computed from cine PC-MRI velocity data obtained under resting conditions. They report average suprarenal shear stress values of  $6.3 \pm 0.2$  dyn/cm<sup>2</sup> and average infrarenal shear stress values of  $2.8 \pm 0.1$  dyn/cm<sup>2</sup>. We note that our shear stress values, while higher than those obtained by Moore *et al.*<sup>15</sup> *in vitro* and Taylor *et al.*<sup>31</sup> using computational methods, are lower than the values reported by Oshinski *et al.*<sup>18</sup> and Oyre *et al.*<sup>19</sup> using MRI techniques *in vivo*. There are a few possible explanations for these differences. First of all, in the present investigation, we used a 0.5 T open magnet as opposed to the 1.5 T conventional magnets used in previously reported measurements. Consequently, we had a lower image resolution in our studies compared to prior investigations. Second, we utilized different methods to compute shear stress in the abdominal aorta from the velocity data. Our method is based on fitting bicubic Lagrange polynomial functions to the data whereas both Oshinski *et al.*<sup>18</sup> and Oyre *et al.*<sup>19</sup> utilized methods based on linear curve fits.

Pedersen *et al.*<sup>21</sup> reported flow rates in the infrarenal abdominal aorta immediately following supine lower limb exercise at varying intensity levels. At an exercise level of 98 W, they reported that mean heart rate increased from  $65 \pm 7$  beats/min at rest to  $115 \pm 16$  beats/min during exercise (conditions roughly comparable to the increase in heart rate in the present study) and observed an increase in infrarenal abdominal aorta flow from  $1.4 \pm 0.3$  L/min at rest to  $6.4 \pm 0.8$  L/min during exercise. These are similar to our values of  $0.9 \pm 0.4$  L/min at rest and  $5.6 \pm 1.1$  L/min during exercise in the infrarenal aorta.

Note that the ratio of average blood flow rate between exercise and rest is larger than that of average wall shear stress. From pulsatile flow theory, the average wall shear stress in a rigid, circular tube is affected only by the steady component of the flow waveform and therefore average wall shear stress is linearly proportional to average blood flow rate.<sup>34</sup> The ratio discrepancy in our *in vivo* data could therefore be due to exercise-related changes in lumen size, imaging artifacts, and/or nonidealized flow conditions. We did not observe an increase in the average lumen size of the abdominal aorta from rest to exercise. Imaging artifacts, including partial volume and temporal image blurring effects are more pronounced during exercise. In the pixels at the edge of the lumen, blood, arterial wall tissue, and external tissue can all contribute to MR signal. However, since signal from the blood is significantly higher than that from other tissue for these particular scans, the edge pixels exhibit erroneously high magnitude and phase signals. During the exercise acquisitions, greater movement during the

scan may have caused significant image blurring, further exacerbating partial volume effects resulting in less accurate lumen segmentation for the exercise images as compared to the rest acquisitions. While inaccurate lumen boundaries do not affect flow quantification significantly due to low velocity values near the lumen edge, they yield artificially low wall shear stresses. This is due to the fact that on average, the velocity gradient is largest at the vessel wall, and errors in estimating the position of the wall results in lower wall shear stress. The anticipated underestimation of wall shear stress at exercise may explain the fact that the ratio of average blood flow rate between exercise and rest is larger than that of average wall shear stress. Nonidealized velocity profiles could also explain the flow and wall shear stress ratio discrepancies. In contrast to assumptions required in pulsatile flow theory, the human abdominal aorta is distensible, has branch vessels, and curves and tapers along the length.

It is also of interest to note that blood flow to the digestive and renal circulations decreased during exercise. This is consistent with observations in the exercise physiology literature, but our results are the first to quantify this reduction in flow *in vivo* during dynamic exercise.

A limitation of this experimental investigation is that hemodynamic conditions were characterized at only two discrete locations in the abdominal aorta. Combined computer modeling<sup>33</sup> and magnetic resonance imaging studies as well as new cine 3DPC (i.e., four-dimensional) MRI sequences<sup>5</sup> have the potential to provide a more complete description of abdominal aortic hemodynamic conditions.

The measured effect of exercise on reducing flow oscillations, increasing wall shear stress and reducing shear stress oscillations in the lesion-prone infrarenal aorta supports the postulate that exercise provides local benefit in portions of the vasculature by eliminating hemodynamic conditions known to correlate with the location of atherosclerotic plaques. It remains to be determined whether these acute changes in hemodynamic conditions have an observed long-term effect on vascular biologic processes hypothesized to be important in inhibiting atherogenesis. Further insights in the effects of exercise on vascular hemodynamics and resultant biologic changes could aid in the development of preventive measures to combat atherosclerosis.

#### ACKNOWLEDGMENTS

The authors gratefully acknowledge the assistance of Anna McVittie and Mary Draney in the Department of Mechanical Engineering, and Dr. Thomas Brosnan, Claudia Cooper, and Ann Taylor in the Department of Radiology at Stanford University. Magnetic resonance imag-

ing time was provided by the Richard M. Lucas Center for Magnetic Resonance Imaging at Stanford.

#### REFERENCES

- <sup>1</sup>Caro, C. G., J. M. Fitz-Gerald, and R. C. Schroter. Atheroma and arterial wall shear: Observation, correlation and proposal of a shear dependent mass transfer mechanism for atherogenesis. *Proc. R. Soc. London, Ser. B: Biological Sciences* 177:109–159, 1971.
- <sup>2</sup>Cheng, C. P., D. Parker, and C. A. Taylor. Wall shear stress quantification from magnetic resonance imaging data using lagrangian interpolation functions. In: Proceedings of the 2001 ASME Summer Bioengineering Meeting. Park City, UT, 2001, pp. 795–796.
- <sup>3</sup>Cheng, C. P., D. Parker, and C. A. Taylor. Quantification of wall shear stress in large blood vessels using Lagrangian interpolation functions with Cine PC-MRI. *Ann. Biomed. Eng.* (submitted).
- <sup>4</sup>Cybulsky, M. I., and M. A. Gimbrone, Jr. Endothelial expression of a mononuclear leukocyte adhesion molecule during atherogenesis. *Science* 251:788–791, 1991.
- <sup>5</sup>Fredrickson, J. O., P. Irrarrazabal, and N. J. Pelc. Quantitative 3d time-resolved phase contrast MR imaging. SMR Workshop: Cardiovascular MRI: Present and Future, 1994, p. 25.
- <sup>6</sup>Fredrickson, J. O., H. Wegmuller, R. J. Herfkens, and N. J. Pelc. Simultaneous temporal resolution of cardiac and respiratory motion in MR imaging. *Radiology* 195:169–175, 1995.
- <sup>7</sup>Friedman, M. H., G. M. Hutchins, and C. B. Barger. Correlation between intimal thickness and fluid shear in human arteries. *Atherosclerosis (Berlin)* 39:425, 1981.
- <sup>8</sup>Glagov, S., D. A. Rowley, and R. Kohut. Atherosclerosis of human aorta and its coronary and renal arteries. *Arch. Pathol. Lab. Med.* 72:558, 1961.
- <sup>9</sup>He, X., and D. Ku. Pulsatile flow in the human left coronary artery bifurcation: Average conditions. *J. Biomech. Eng.* 118:74–82, 1996.
- <sup>10</sup>Ku, D., D. Giddens, C. Zarins, and S. Glagov. Pulsatile flow and atherosclerosis in the human carotid bifurcation: Positive correlation between plaque location and low oscillating shear stress. *Atherosclerosis (Berlin)* 5:293–302, 1985.
- <sup>11</sup>Moore, J., D. Ku, C. Zarins, and S. Glagov. Pulsatile flow visualization in the abdominal aorta under differing physiologic conditions: Implications for increased susceptibility to atherosclerosis. *J. Biomech. Eng.* 114:391–397, 1992.
- <sup>12</sup>Moore, J., and D. Ku. Pulsatile velocity measurements in a model of the human abdominal aorta under resting conditions. *J. Biomech. Eng.* 116:337–346, 1994.
- <sup>13</sup>Moore, J., and D. Ku. Pulsatile velocity measurements in a model of the human abdominal aorta under simulated exercise and postprandial conditions. *J. Biomech. Eng.* 116:107–111, 1994.
- <sup>14</sup>Moore, J., S. Maier, D. Ku, and P. Boesiger. Hemodynamics in the abdominal aorta: a comparison of *in vitro* and *in vivo* measurements. *J. Appl. Physiol.* 76:1520–1527, 1994.
- <sup>15</sup>Moore, Jr., J. E., C. Xu, S. Glagov, C. K. Zarins, and D. N. Ku. Fluid wall shear stress measurements in a model of the human abdominal aorta: Oscillatory behavior and relationship to atherosclerosis. *Atherosclerosis (Berlin)* 110:225–240, 1994.
- <sup>16</sup>Niezen, R. A., J. Doornbos, E. E. Van Der Wall, and A. De Roos. Measurement of aortic and pulmonary flow with MRI

- at rest and during physical exercise. *J. Comput. Assist. Tomog.* 22:194–201, 1998.
- <sup>17</sup>Nobutaka, I., S. Ramasamy, T. Fukai, R. Nerem, and D. G. Harrison. Shear stress modulates expression of Cu/Zn superoxide dismutase in human aortic endothelial cells. *Circ. Res.* 79:32–37, 1996.
- <sup>18</sup>Oshinski, J. N., D. N. Ku, S. Mukundan, Jr., F. Loth, and R. I. Pettigrew. Determination of wall shear stress in the aorta with the use of MR phase velocity mapping. *Magn. Reson. Imaging* 5:640–647, 1995.
- <sup>19</sup>Oyre, S., E. M. Pedersen, S. Ringgaard, P. Boesiger, and W. P. Paaske. *In vivo* wall shear stress measured by magnetic resonance velocity mapping in the normal human abdominal aorta. *Eur. J. Vasc. Endo. Surg.* 13:263–271, 1997.
- <sup>20</sup>Pedersen, E. M., S. Hsing-Wen, A. C. Burlson, and A. P. Yoganathan. Two-dimensional velocity measurements in a pulsatile flow model of the normal abdominal aorta simulating different hemodynamic conditions. *J. Biomech.* 26:1237–1247, 1993.
- <sup>21</sup>Pedersen, E. M., S. Kozerke, S. Ringgaard, M. B. Scheidegger, and P. Boesiger. Quantitative abdominal aortic flow measurements at controlled levels of ergometer exercise. *Magn. Reson. Imaging* 17:489–494, 1999.
- <sup>22</sup>Pelc, L. R., N. J. Pelc, S. C. Rayhill, L. J. Castro, G. H. Glover, R. J. Herfkens, D. C. Miller, and R. B. Jeffrey. Arterial and venous blood flow: Noninvasive quantitation with MR imaging. *Radiology* 185:809–812, 1992.
- <sup>23</sup>Pelc, N. J., F. G. Sommer, K. C. Li, T. J. Brosnan, R. J. Herfkens, and D. R. Enzmann. Quantitative magnetic resonance flow imaging. *Magn. Reson. Q.* 10:125–147, 1994.
- <sup>24</sup>Pollack, M., and J. Wilmore. *Exercise in Health and Disease: Evaluation and Prescription for Prevention and Rehabilitation*, 2nd ed. Philadelphia: W. B. Saunders, 1990.
- <sup>25</sup>Roberts, J. C., C. Moses, and R. H. Wilkins. Autopsy studies in atherosclerosis: I. Distribution and severity of atherosclerosis in patients dying without any morphologic evidence of atherosclerotic catastrophe. *Circulation* 20:511–519, 1959.
- <sup>26</sup>Schalet, B., C. Taylor, E. Harris, R. Herfkens, and C. Zarins. Quantitative assessment of human aortic blood flow during exercise. *Surg. Forum.* XLVIII:359–362, 1997.
- <sup>27</sup>Sessa, W., K. Pritchard, N. Seydi, J. Wang, and T. Hintze. Chronic exercise in dogs increases coronary vascular nitric oxide production and endothelial cell nitric oxide synthase gene expression. *Circ. Res.* 74:349–353, 1994.
- <sup>28</sup>Sethian, J. A. *Level Set Methods and Fast Marching Methods*. Cambridge: Cambridge University Press, 1999.
- <sup>29</sup>Strong, J. P., G. T. Malcom, C. A. McMahan, R. E. Tracy, W. P. Newman III, E. E. Herderick, and J. F. Cornhill. Prevalence and extent of atherosclerosis in adolescents and young adults: Implication for prevention from pathobiological determinants of atherosclerosis in youth study. *J. Am. Med. Assoc.* 281:727–735, 1999.
- <sup>30</sup>Taylor, C. A., T. J. R. Hughes, and C. K. Zarins. Finite element modeling of three-dimensional pulsatile flow in the abdominal aorta: Relevance to atherosclerosis. *Ann. Biomed. Eng.* 26:975–987, 1998.
- <sup>31</sup>Taylor, C. A., T. J. R. Hughes, and C. K. Zarins. Effect of exercise on hemodynamic conditions in the abdominal aorta. *J. Vasc. Surg.* 29:1077–1089, 1999.
- <sup>32</sup>Wang, J., S. M. Wolin, and H. T. Hintze. Chronic exercise enhances endothelium-mediated dilation of epicardial coronary artery in conscious dogs. *Circ. Res.* 73:929–1838, 1993.
- <sup>33</sup>Wang, K. C., R. W. Dutton, and C. A. Taylor. Geometric image segmentation and image-based model construction for computational hemodynamics. *IEEE Eng. Med. Biol. Mag.* 18:33–39, 1999.
- <sup>34</sup>Womersley, J. Method for the calculation of velocity, rate of flow and viscous drag in arteries when the pressure gradient is known. *J. Physiol. (London)* 127:553–563, 1955.
- <sup>35</sup>Zarins, C. K., R. A. Bomberger, and S. Glagov. Local effects of stenoses: Increased flow velocity inhibits atherogenesis. *Circulation* 64:II-221–227, 1981.
- <sup>36</sup>Zarins, C. K., D. P. Giddens, B. K. Bharadvaj, V. S. Sottiurai, R. F. Mabon, and S. Glagov. Carotid bifurcation atherosclerosis: Quantitative correlation of plaque localization with flow velocity profiles and wall shear stress. *Circ. Res.* 53:502–514, 1983.